

Nanomechanical Forces Generated by Surface Grafted DNA

Michael F. Hagan,^{†,||} Arun Majumdar,^{‡,||} and Arup K. Chakraborty^{*,†,§,||,⊥}

Department of Chemical Engineering, Department of Mechanical Engineering, and Department of Chemistry, University of California, Berkeley, California 94720, and Materials Science Division and Physical Biosciences Division, Lawrence Berkeley National Laboratory, Berkeley, California 94720

Received: April 15, 2002; In Final Form: July 1, 2002

Recent experiments show that the adsorption of biomolecules on one surface of a microcantilever generates surface stresses that cause the cantilever to deflect. If a second species binds to the adsorbed molecules, the stresses change, resulting in a different deflection. By choosing adsorbed probe molecules that recognize specific molecules, it may be possible to detect pathogens and biohazards. In particular, Fritz et al. (Fritz, J.; Baller, M. K.; Lang, H. P.; Rothuizen, H.; Vettiger, P.; Meyer, E.; Guntherodt, H.-J.; Gerber, Ch.; Gimzewski, J. K. *Science* **2000**, 288, 316) and Wu et al. (Wu, G.; Haifeng, J.; Hansen, K.; Thundat, T.; Datar, R.; Cote, R.; Hagan, M. F.; Chakraborty, A. K.; Majumdar, A. *Proc. Natl. Acad. Sci. U.S.A.* **2001**, 98, 1560) show that the presence of an individual sequence of DNA may be identified by observing the change in deflection as hybridization occurs. Also, it has been shown that this platform can detect prostate specific antigen (PSA). However, to exploit this phenomenon for the development of reliable microdevices, it is necessary to understand the origin of the nanomechanical forces that lead to cantilever deflection upon molecular recognition, as well as the dependence of such deflections on the identity and concentration of the target molecule. In this paper, we present a model with which we examine cantilever deflections resulting from adsorption and subsequent hybridization of DNA molecules. Using an empirical potential, we predict deflections upon hybridization that are consistent with experimental results. We find that the dominant contribution to these deflections arises from hydration forces, not conformational entropy or electrostatics. Cantilever deflections upon adsorption of single stranded DNA are smaller than those predicted after hybridization for reasonable interaction strengths. This is consistent with results in Fritz et al., but not those in Wu et al. The deflections predicted for DNA before and after hybridization are strongly dependent on surface coverage, as well as the degree of disorder on the surface. We argue that self-assembly of probe molecules on the cantilever surface must be carefully controlled and characterized for the realization of microdevices for pathogen detection that rely on nanomechanical forces generated by molecular recognition.

1. Introduction

Developing the capability to identify molecules that act as pathogens, cancer indicators, chemical weapons, or biohazards is important for the health care industry and national security. Many approaches to this end are being explored. We are considering a tactic that is motivated by recent experiments.^{1–4} In these experiments, a group of identical “probe” molecules are end-attached to one surface of a microcantilever beam (Figure 1). Experiments^{1–4} find that this causes the cantilever to bend, or deflect. The deflection is measured optically. A solution containing “target” molecules, or molecules that can bind to the probe, is then introduced. Experiments show that, upon binding, the deflection changes. Results from these experiments suggest that the identity, and sometimes concentration, of the target molecule is related to the change in deflection. Thus, we envision a microarray of cantilevers, each of which has a different probe molecule immobilized on the active surface. When a fluid sample enters such a microfluidic device, the deflection of each cantilever is monitored separately. The

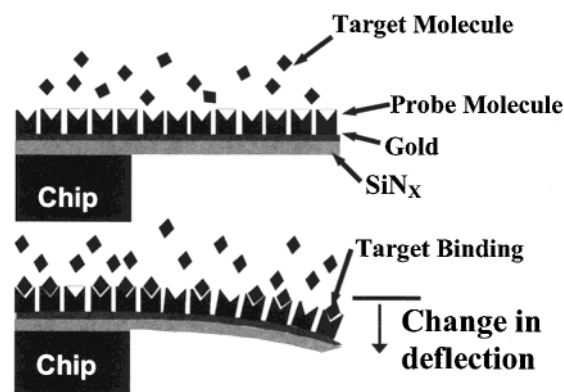


Figure 1. Basic platform used for experiments performed in Wu et al.²

fluid sample can then be screened for target molecules based on the change in deflection of each cantilever.

Development of this system will involve designing, for each target of interest, a probe–target–cantilever system that yields observable and reproducible deflections. This general problem requires the development of a set of design rules that translate molecular-scale binding and recognition to measurable responses of a microdevice. In particular, we need to understand, at a very fundamental level, the relationship between the nanomechanical

* Corresponding author.

[†] Department of Chemical Engineering, University of California.

[‡] Department of Mechanical Engineering, University of California.

[§] Department of Chemistry, University of California.

^{||} Materials Science Division, Lawrence Berkeley National Laboratory.

[⊥] Physical Biosciences Division, Lawrence Berkeley National Laboratory.

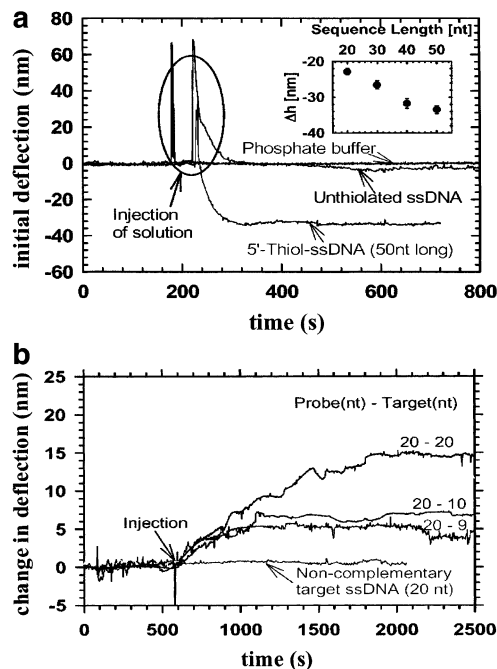


Figure 2. Typical result from experiments in Wu et al.² (a) Deflection vs time upon immobilization of ssDNA. (b) Change in deflection vs time as hybridization takes place. (Figure taken from Figures 2a and 3a in Wu et al.²)

forces generated by molecular binding and the characteristics of the target and probe molecules.

Modeling such a system in its entirety, and developing the pertinent design rules, necessitates a hierarchy of simulation methods and theories that span different length and time scales. These computational studies must be carried out in close synergy with experiments which probe the same phenomena. The first step in developing hierarchical methods aimed toward modeling these systems is to develop an understanding of the forces that govern the deflections of one cantilever upon immobilization of the probe molecules and probe–target complexes. This paper will concentrate on cantilever deflection at equilibrium. We will focus on analyzing experiments that involve DNA hybridization. It is worth remarking, however, that the experimental platform under consideration can be used to detect other biological molecules. For example, Wu et al.³ have demonstrated its applicability to measurement of prostate specific antigen (PSA) at concentration levels that are clinically relevant for diagnosis of prostate cancer.

In the experiments involving DNA, a solution containing end-thiolated single stranded DNA (ssDNA) molecules (the probe molecules) is introduced into a cell containing a silicon nitride (Si_3N_4) cantilever, which has one surface coated with gold. The ssDNA molecules end adsorb on the gold surface of the cantilever through the strong gold–thiol bond. Then, a solution containing the complementary strands of ssDNA (the target molecules) is introduced and the change in deflection is measured as probe–target hybridization takes place. An example of the data resulting from such an experiment is given in Figure 2.

These experiments have been carried out by different groups in slightly different conditions, with significantly different results. In Fritz et al.¹ ssDNA was immobilized in 50 mM triethylammonium acetate buffer with 25% ethanol, while hybridization reactions were carried out in saline sodium citrate hybridization buffer. It was found that cantilever deflection increased upon hybridization. In Wu et al.,² DNA was im-

mobilized and subsequently hybridized in sodium phosphate buffer (PB) at concentrations ranging from 0.1 to 1 M. In these cases, hybridization caused a reduction in deflection. However, when immobilization was performed at 1 M PB, but hybridization was carried out in 0.1 M PB, the deflection increased upon hybridization. In all experiments the pH was maintained at about 7.0.

Thus far, the mechanisms responsible for the cantilever deflection upon immobilization and hybridization of DNA have been considered only in a limited and qualitative way. Fritz et al.¹ suggested that electrostatics and steric interactions among immobilized molecules lead to a surface strain which causes cantilever deflection. Hybridization increases the magnitude of these interactions and thus increases the deflection. In Wu et al.² it is suggested that the steric and electrostatic effects are coupled to configurational entropy. Because ssDNA has a much shorter persistence length ($l_p \approx 0.75$ nm) than double stranded DNA (dsDNA; $l_p \approx 50$ nm),⁵ configurational entropy effects are assumed to be much larger for ssDNA. Therefore, it is suggested that the negative change in deflection upon hybridization results from the decrease in importance of configurational entropy. Thus far, neither assertion has been investigated in a meaningful way.

In this paper, we describe systematic computational studies of cantilever deflection resulting from end-adsorbed molecules. Specifically, we study double stranded DNA and flexible macromolecules that serve as a model for single stranded DNA. Comparison of our results with experiments sheds light on the important physical processes involved in the generation of nanomechanical forces upon DNA hybridization. Our studies also highlight the importance of a basic lack of understanding of how ssDNA molecules interact with each other and with water. [This deficiency can, in principle, be addressed through atomistically detailed calculations (see, e.g., ref 6). However, with current computational resources the extent of such calculations is limited, so we concentrate on coarse grained investigations in this paper.] Our calculations, in conjunction with experiments, also point to the importance of careful control and characterization of adsorbed layers of probe molecules. We find that this is necessary for consistent interpretation of experiments in different laboratories and, ultimately, for the design of reliable microdevices. For example, we find that small amounts of disorder in the adsorbed layer can significantly affect cantilever deflection.

This paper is organized as follows. In section 2, we describe the basic models that we employ to study the pertinent phenomena and present our main results. In section 3 we summarize the important findings and discuss new experiments that these findings suggest.

2. Model and Description of Results

2.1. Overall Free Energy. In our model, the forces determining equilibrium cantilever deflection can be divided into four basic categories. First, the conformational entropy of an adsorbed macromolecule is decreased by the presence of neighboring molecules. The molecules also energetically repel each other, due to solvent-mediated interactions as well as electrostatic repulsions. We will represent the electrostatic free energy by F_{ELEC} , and the free energy resulting from macromolecular conformational entropy and nonelectrostatic interactions will be denoted by F_{POLY} . In addition, there is a free energy contribution associated with the osmotic pressure of the counterions localized in the region of the cantilever due to the charges on DNA molecules. This will be denoted by F_{OSM} . The free energy

associated with these effects decreases as the intermolecular distances and volume occupied by counterions increase. In other words, adsorption on a curved surface leads to lower free energies for the same average distance between molecular graft points on the surface. In the cantilever experiments, these effects lead to a force that favors deflection. There is, however, a mechanical energy penalty associated with bending the cantilever, denoted by E_{CANT} . The balance between these two effects determines the cantilever deflection at equilibrium. E_{CANT} can be expressed as⁷

$$E_{\text{CANT}} = \frac{C}{R^2} \quad (1)$$

where C depends on the thickness of the cantilever and the modulus of the material of construction and R denotes the radius of curvature of the shape adopted by the cantilever.

The overall free energy, F , can now be written as

$$F = E_{\text{CANT}} + F_{\text{POLY}} + F_{\text{OSM}} + F_{\text{ELEC}} \quad (2)$$

If we are able to determine the dependence of the latter three terms on R , then the equilibrium radius, R_{EQ} , can be calculated by minimizing $F(R)$. In the limit of small curvature, the optically measured deflection (δ) is then given by

$$\delta = \frac{d_2^2}{2R_{\text{EQ}}}, \quad (3)$$

where d_2 is the length of the cantilever. All deflections given in this paper are given for the cantilever used in Wu et al.,² with $d_2 = 200 \mu\text{m}$ and $C = 10^{-9} \text{ J}$. Using the following formula, however, C , and thus deflections, can be determined for any cantilever:⁷

$$C = \frac{Ed_1^3}{24R^2(1 - \nu_c^2)} \quad (4)$$

where d_1 is the thickness of the cantilever, E is Young's modulus, and ν_c is the Poisson ratio. For the cantilever used by Wu et al.,² $d_1 = 500 \text{ nm}$, $E = 180 \text{ Pa}$, and $\nu_c = 0.25$.

2.2.a. Model for Immobilized Semiflexible Polymers (dsDNA). The methods used to estimate the free energy contributions to eq 2 depend on the specific molecular system. The form of the terms in eq 2 other than E_{CANT} are thus different for a flexible molecule such as ssDNA which has a persistence length that is smaller than any average distance between grafting points we will consider, and a semiflexible molecule, such as dsDNA, whose persistence length is orders of magnitude larger. For simplicity we have assumed a hybridization efficiency of 100% (thus all immobilized DNA is double stranded after the hybridization step). We note, however, that the actual hybridization efficiency may be significantly smaller at high grafting densities.⁸

Due to its importance in biology, much effort has gone into describing various properties of dsDNA. In a set of experiments that is particularly relevant to this work, Parsegian and co-workers laterally compressed hexagonally ordered arrays of aqueous dsDNA.⁹⁻¹³ The necessary force was measured as a function of distance between chains and salt concentration. These measurements were fit to expressions based on theories for nematicity ordered semiflexible polymers to obtain an effective pairwise interaction potential between dsDNA molecules.⁹⁻¹² We briefly summarize the relevant findings.

Molecules of dsDNA resist lateral compression due to electrostatic interactions and hydration forces. The electrostatic repulsions (per unit length) between two cylinders with an effective charge per length, l_e , located on the outside of the cylinder can be written as^{9,14}

$$F_{\text{EL}} = f_0 \sqrt{\frac{\pi}{2}} \frac{\exp(-d/\lambda_D)}{\sqrt{d/\lambda_D}} \quad (5)$$

where

$$f_0 = \frac{2kTl_b}{\left(l_e \frac{a}{\lambda_D} K_1\left(\frac{a}{\lambda_D}\right)\right)^2} \quad (6)$$

and l_b denotes the Bjerrum length (7.14 Å in water). The radius of dsDNA (about 1 nm) is denoted by a . The value of l_e depends on the degree to which counterions condense on the DNA (see, e.g., ref 15), also known as Manning condensation. In Strey et al.⁹ it is suggested that the degree of Manning condensation in these DNA systems is smaller than that predicted by conventional counterion condensation theory; thus l_e may be smaller than l_b (also see Hansen et al.¹⁶).

Hydration forces result from perturbation of the hydrogen bonding network in water by the DNA molecules.¹⁷ In particular, dsDNA is surrounded by at least two hydration shells which contain about 20 water molecules per base pair.¹⁸ This results in a strongly repulsive force as DNA molecules are brought together. Leiken et al.¹⁷ suggest that the free energy per unit length (F_{H}) resulting from hydration forces between cylinders should be written in a form similar to the electrostatic repulsions:

$$F_{\text{H}} = b \sqrt{\frac{\pi}{2}} \frac{\exp(-d/\lambda_H)}{\sqrt{d/\lambda_H}} \quad (7)$$

where λ_H is the correlation length of water ($\approx 0.3 \text{ nm}$) and b must be determined empirically.

In an array of semiflexible molecules such as those used in the experiments,⁹⁻¹³ the bare interaction forces given by eqs 5 and 7 are renormalized by conformational fluctuations.⁹⁻¹² Based on an analysis of nematicity ordered polymers, Strey et al.⁹ show that the effective free energy as a function of axial separation can be written as

$$F(d) = F_0(d) + ck_B T k_c^{-1/4} \sqrt{\frac{\partial^2 F_0}{\partial d^2} - \frac{1}{d} \frac{\partial F_0}{\partial d}} \quad (8)$$

where $F_0 = F_{\text{H}} + F_{\text{EL}}$ and k_c denotes the bending stiffness ($k_c = k_B T l_p$). The parameter c is a dimensionless constant (of order 1) that was fit to experimental data in Strey et al.⁹

As the distance between chains is increased, F_0 decays exponentially with the decay length, λ . For the second term in eq 8 (the fluctuation effect) the decay length is effectively quadrupled. Thus, at large distances, the observed decay length is 4λ (which has been seen experimentally⁹). At interaxial distances below 3.2 nm, the decay length was found to be approximately 0.3 nm, regardless of buffer concentration, indicating hydration forces dominated at all measured salt concentrations (0.1–2 M NaCl). Hydration forces are so strong below this separation distance that fluctuations are suppressed (as seen with X-ray diffraction⁹) and the first term in eq 8 dominates.

The experimental force vs distance measurements are fit to eq 8 in Strey et al.⁹ This gives a pairwise potential per unit length for dsDNA molecules as a function of molecular separation, $w(d;[\text{Na}^+])$, where the salt concentration is a parameter. We can use this to directly predict deflection for immobilized dsDNA, provided we first address two differences between the cantilever experiments and the model experiments in Strey et al.⁹ While DNA molecules are hexagonally ordered in the experiments in Strey et al.,⁹ chains are adsorbed on the cantilever surface in an unknown pattern that is likely very disordered. We consider the effect of disorder in section 2.2.b. Second, the analysis of fluctuations for nematic systems that leads to eq 8 is only applicable to long chains; at the very least the chains should be longer than the persistence length, l_p . The persistence length of dsDNA (~ 50 nm)⁵ is significantly longer than the contour length of any of the chains used in the cantilever experiments. Although this should make the reader question the applicability of the above analysis to the cantilever experiments, it does not necessarily imply that there are no fluctuation effects in these chains. Due to the exponential nature of the bare forces, small deviations from the straight conformation can lead to significant fluctuation-induced effects in this system. Analysis in Podgornik et al.^{11,12} suggests that the axial length over which these fluctuations take place is only about 4 nm, which is less than the contour lengths of the DNA molecules used in the experiments. Thus, at sufficiently low grafting densities, there most likely are fluctuation effects in the cantilever experiments and we used the full form of eq 8 in our analysis. Based on our findings and experiments,¹⁹ we believe that the pertinent surface coverages are above the threshold at which fluctuations are suppressed due to strong hydration forces. Therefore, the part of eq 8 that is not applicable to short chains did not significantly contribute to our predictions.

Deflections are predicted as follows. We assume the molecules are grafted in an ordered fashion, with the mean interaxial distance at the cantilever surface given by $d_0 \cong 1/\sigma^{1/2}$, where σ denotes the grafting density. Due to curvature of the cantilever, the distance between DNA molecules, $d(s)$, increases with radial distance from surface, s . In the limit of small curvature, the variation is given by

$$d(s) = d_0 \left(1 + \frac{s}{R} \right) \quad (9)$$

The free energy per unit area, which includes both the polymer free energy and electrostatic effects is then approximately given by

$$F_{\text{OSM}} + F_{\text{POLY}} + F_{\text{ELEC}} = \sigma \int_0^{L_c} w[d(s);[\text{Na}^+]] ds \quad (10)$$

In the limit of small curvatures, we can expand quantities to first order in L_c/R and minimize the total free energy (eq 2) to obtain an analytical expression for cantilever deflection. The resulting expression is

$$\delta = \frac{L_c^2 \frac{\partial F}{\partial d} \Big|_{d_0}}{8Cd_0} \quad (11)$$

2.2.b. Results for Double Stranded DNA (Semiflexible Polymers). The variation of deflection with grafting density and chain length predicted using this approach is shown in Figure 3. We cannot compare these results to the data in Frtiz et al.¹ because absolute deflections were not recorded. There is good agreement between the predicted deflections in Figure 3a

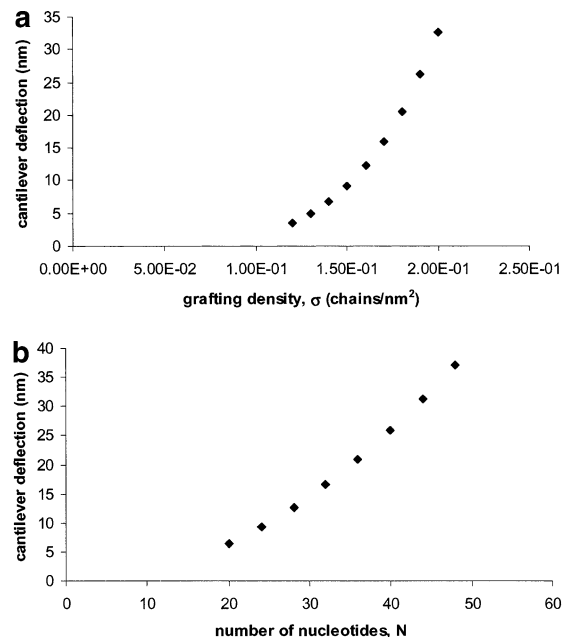


Figure 3. Deflections predicted for dsDNA using empirical potential in Strey et al.¹⁰ (a) Deflections vs grafting density for 30 nucleotide molecule. (b) Deflections predicted for grafting density of 0.17 chains/nm². Results are applicable to solutions with bulk $[\text{Na}^+]$ of 1 M and larger (hydration forces dominate at all grafting densities at or above 1 M $[\text{Na}^+]$, with $b = 1.7 \times 10^{-7}$ J/m, $\lambda = 2.9$ Å, and $c = 1.2$).

and the corresponding experimental values (Figure 3a in Wu et al.²) for grafting densities in the range of 0.15–0.2 chains/nm². These grafting densities are in reasonable agreement with surface coverages reported in a similar system¹⁹ and correspond to intermolecular distances in the range of $d_0 = 2.3$ – 2.6 nm. These intermolecular distances are below the threshold at which fluctuations are suppressed (vide supra).

When obtaining the results shown in Figure 3, we assumed that all molecules were separated by an average distance, $\langle d_0 \rangle$. In reality, the self-assembly of end-adsorbed ssDNA molecules may not be uniform on the scale of a few nanometers, and so the surfaces are most likely disordered on short length scales. We investigated the effect of having a distribution of distances between molecules by calculating cantilever deflections for the following Gaussian distribution of distances, $P(d_0)$:

$$P(d_0) = C_1 \exp \left[-\frac{(d_0 - \langle d_0 \rangle)^2}{2\omega^2} \right] \quad d_0 \geq d_c \quad (12a)$$

$$P(d_0) = 0 \quad d_0 < d_c \quad (12b)$$

where ω is the standard deviation and C_1 is the normalization constant given by

$$C_1^{-1} = \omega \sqrt{\frac{\pi}{2}} \left[\text{erfc} \left(\frac{d_c - \langle d_0 \rangle}{\sqrt{2}\omega} \right) \right] \quad (13)$$

The cutoff, d_c , is imposed because the potential diverges as the separation approaches zero. We chose $d_c = 1$ nm, the radius of dsDNA. As can be seen in Figure 4, relatively small values of the standard deviation can cause dramatic increases in deflection. This is because the exponential dependence of the chain–chain interactions makes the repulsive interactions between chains at separations smaller than $\langle d_0 \rangle$ dominant. Thus, deflections similar to those seen experimentally can be predicted with $\langle d_0 \rangle$ that is greater than 3.2 nm, the distance below which hydration forces begin to dominate. However, the deflection

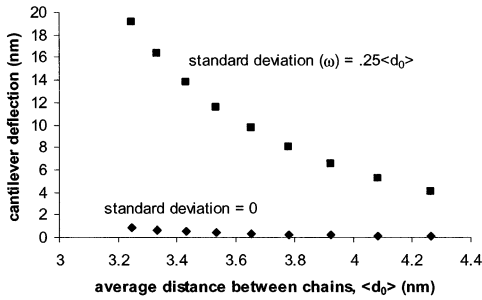


Figure 4. Dependence of predicted deflections for dsDNA as a function of disorder on the surface. Because of the exponential nature of the interactions, a standard deviation of $0.25\langle d_0 \rangle$ is sufficient to increase the predicted deflection by an order of magnitude.

behavior in these cases is dominated by the small distance part of the distribution, and thus the deflections are still relatively insensitive to salt concentration.

This strong dependence of cantilever deflection on disorder has important implications for experimental design of pathogen detection microdevices that employ surface adsorbed probe molecules. The nanoscale self-assembly of adsorbed probe molecules must be carefully controlled for reproducible (and thus, reliable) responses of the microdevice.

2.3.a. Modeling Grafted Flexible Polymers (ssDNA). As mentioned above, there is relatively little information about the segment–segment interactions in ssDNA. In this section, we will discuss several models of flexible polymer chains that are appropriate for different segment–segment interaction strengths. As in the case of modeling dsDNA, some of the methods we will use are strictly valid only in the long chain limit, but we will validate the predictions of these methods by comparing them to results of Monte Carlo simulations (in which case the long chain limit is not directly assumed).

If we assume the interactions are sufficiently weak that they can be approximated by short-ranged excluded volume potentials, we can estimate the polymer free energy by utilizing several methods commonly used to examine polymer brushes, e.g.,^{20–23} scaling laws, self-consistent-field (SCF) methods, and Monte Carlo (MC) simulations.

The effects of curvature in polymer brushes were first analyzed through scaling laws by Daoud and Cotton²⁴ and later by Halperin.²⁵ For a cylinder this approach yields

$$F_{\text{POLY}} = 2R\sigma^{3/2} \left[\left(1 + \frac{Nl(\sigma v)^{1/3}}{R} \right)^{3/8} - 1 \right] \quad (14)$$

where the height of the brush (L) is given by

$$\left(\frac{L}{R} + 1 \right)^{4/3} = 1 + \frac{Nl(\sigma v)^{1/3}}{R} \quad (15)$$

N denotes the chain length, l is the statistical segment length ($l \approx 2l_p$), σ is the grafting density, and v is the excluded volume, which must be treated as a fitting parameter. Unless otherwise noted, we have taken the intrinsic statistical segment length of ssDNA to be $l = 1.5$ nm,⁵ although other estimates exist (e.g., $l \approx 2$ nm in Tinland et al.²⁶). In the case of neutral chains, F_{OSM} and F_{ELEC} do not contribute, and the following expression results for the equilibrium deflection:

$$\delta = \frac{d_2^2 (15/64) \sigma^{13/6} (v/l)^{2/3} L_C^2}{4C} \quad (16)$$

This expression is similar to the result derived in Hiergeist and

Lipowsky²⁷ for the influence of grafted polymers on the effective bending modulus of a membrane.

This approach has been extended to polyelectrolyte brushes by relating the persistence length and excluded volume parameter to the local concentrations of charges within the brush (e.g., Pincus²⁸ and Hariharan et al.²⁹). We will follow Hariharan et al.²⁹ and assume both effects are accounted for by the following relation:

$$v = l^2 \kappa^{-1} \quad (17)$$

where κ^{-1} is the local Debye length (≈ 0.3 nm/ $C_S^{1/2}$), with C_S denoting the local salt concentration.

To establish the appropriate value of κ to set the excluded volume parameter, as well as to estimate the contributions of F_{OSM} and F_{ELEC} , we must determine the densities of the neutralizing counterions within the brush. However, the ionic densities (and therefore the electric potential) depend on local polymer concentrations, and thus are coupled to the polymer conformations. These dependencies are further coupled through eq 17, rendering an analytical solution infeasible. In the following calculation, the ionic concentrations are approximately determined according to a method suggested in Hariharan et al.²⁹ the spatial variations of charge density and electric potential within the brush are neglected and mean values are considered. With the assumption of electroneutrality in the brush, the mean ionic concentrations can be related to the mean electric potential using the Poisson–Boltzmann (PB) equation. This calculation follows directly from Hariharan et al.,²⁹ with appropriate modifications for a cylindrical system. We then assume the molecular volumes for the solvent molecules and the counterions are the same, denoted by v , and calculate the mixing free energy of the counterions and solvent, F_{MIX} . Since the system is in equilibrium with bulk solution, the appropriate free energy is actually the excess free energy, which was earlier denoted by F_{OSM} :

$$F_{\text{OSM}} = F_{\text{MIX}} - \sum_i \mu_i n_i^{\text{tot}} = \int_V \sum_i n_i \ln \frac{n_i}{n_i^\infty} \frac{dV}{v} \quad (18)$$

where μ_i and n_i^{tot} denote the chemical potential and total number of molecules of species i . The number fraction of species i within the brush and in bulk are denoted by n_i and n_i^∞ , respectively. The summation runs over the counterions ($i = 1, 2$) and solvent molecules ($i = 3$). In the cylindrical geometry appropriate for the cantilever experiments, this yields

$$F_{\text{OSM}} = \frac{Nv_p\sigma}{z} \ln Q + \left(Nl + \frac{(Nl)^2 n_3}{2R} \right) \frac{n_3}{v} \ln \frac{n_3}{n_3^\infty} \quad (19)$$

with

$$Q = \left[1 + \left(\frac{\bar{\rho}_P}{2ezn_1^\infty} \right)^2 \right]^{1/2} - \frac{\bar{\rho}_P}{2ezn_1^\infty} \quad (20)$$

where $\bar{\rho}_P$ denotes the density of polymer charges:

$$\bar{\rho}_P = \frac{1}{V} \int_V \rho_P dV = -z \sum_{i=1,2} en_i \quad (21)$$

and z denotes the valence of the electrolyte (assumed to be symmetric: $z = z_1 = -z_2$ and $n_1^\infty = n_2^\infty$). In eq 19, v_p denotes the amount of charge per polymer segment. Except where indicated otherwise in this paper, we have assumed full Manning

condensation, which implies the upper limit of v_P is

$$v_P = \frac{l}{l_b} \quad (22)$$

where l_b is the Bjerrum length. The first term in eq 19 represents the contribution of the ions, and the second term comes from the entropy of the solvent.

In the preceding development, the concentration and free energy of the counterions are determined without accounting for excluded volume. In other words, the counterion free energy is that of an ideal gas. Furthermore, the polymer and ion concentrations are not allowed to vary within the brush.²⁹ Both of these assumptions can be relaxed using the discretized SCF method of Scheutjens and Fleer²³ (SF). We have performed SF calculations that account for electrostatic effects³⁰ and variations in chain flexibility.³¹ Except where otherwise mentioned, conformations which include back-folding are not counted and effects of bond correlations are included.³¹

Since the DNA molecules used in the experiments of concern are short, and because we do not expect scaling laws or the SF calculations to be applicable in the limit of strong or long-ranged segment–segment interactions, we carried out complementary MC simulations. In the MC simulations discussed in this paper, a molecule is represented by a chain of spheres, each of which has an adjustable interaction potential, $u(r)$. The potential included a term to represent hard sphere interactions, u_{HS} , as well as a term appropriate for both electrostatic and hydration forces in three dimensions:

$$u(r) = u_{HS} + u_0 \frac{\exp(-r/\lambda)}{r} \quad (23)$$

In the case of electrostatics the prefactor is given by

$$u_0 = \frac{f^2 e^2}{\epsilon} \quad (24)$$

where f is the number of charges per segment, e is the charge of an electron, and ϵ is the dielectric constant. In the case of hydration forces, we cannot make an a priori estimate for the magnitude of u_0 , but we assume that the decay length (λ) is related to the correlation length of water (as it is for dsDNA). Flexibility is adjusted by regulating the number of “freely rotating” spheres. A freely rotating sphere can form any bond angle, whereas all other spheres are restricted to bond angles of 180° . In this way, the statistical segment length can be adjusted from one bead to the entire molecule (a rod).

Chain conformations are generated using the configurational bias method,³² and free energies are estimated using Frenkel’s modification of the Widom insertion method.³² Except where otherwise mentioned, one sphere represents a statistical segment of ssDNA. The grafting points are annealed in most simulations. It is likely that grafting locations of the chains in the experiments are quenched on experimental time scales. We also carried out simulations with quenched graft points (this requires a slight modification to Frenkel’s algorithm). The results for quenched graft points were qualitatively the same as the results we will discuss.

2.3.b. Results for Flexible Polymers with Weak Interactions. We first investigate neutral chains with only hard sphere interactions. Figure 5a shows the deflections found in MC simulations at different chain lengths (N), normalized by N^2 . The chain length scaling is made evident by the fact that the

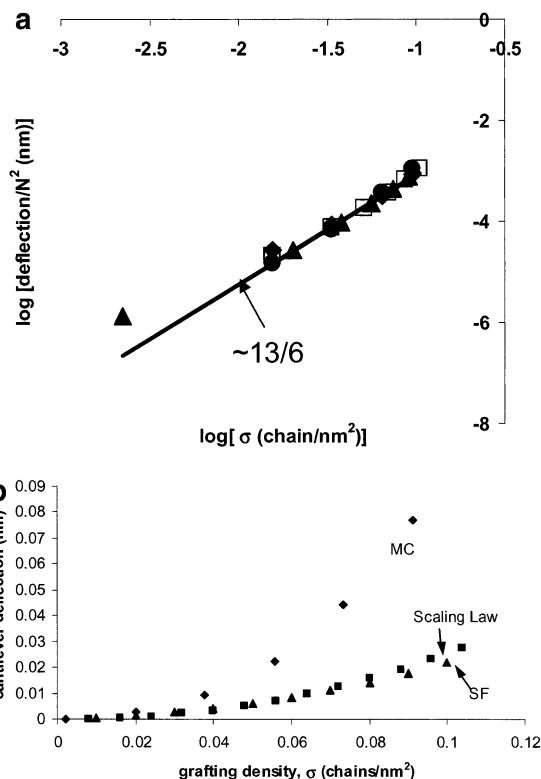


Figure 5. Deflections for athermal chains. (a) Deflections from athermal MC simulations match scaling law (eq 16). Results are from MC simulations at $N = 5$ (\blacklozenge), 7 (\blacksquare), 10 (\blacktriangle), and 15 (\bullet) segments. If we assume a statistical segment length of 1.5 nm, this corresponds to 13 – 38 nt. Normalizing the deflections by N^2 causes all results to collapse onto a single curve. The solid line corresponds to $\delta \sim \sigma^{13/6}$. (b) Absolute deflections for athermal chains using MC simulations, SF calculations, and the scaling law. Results are shown for a chain of 10 segments (≈ 25 nt). These are well below the experimental deflections ($\delta \approx 20$ – 30 nm) [see Figure 2a in Wu et al.²]. Results from both MC simulations and SF calculations show similar scaling, but the MC deflections are about twice as large as results from the other two methods. Unlike the other results for SF calculations in this paper, flexibility effects (along with bond correlation and back-folding effects) were not included in this SF calculation. This was to keep the excluded volume at $v = P^3$ as it is in the MC simulations and scaling law calculation. Except where otherwise noted, all SF calculations were performed with the Flory χ parameter set to zero.

results collapse on to one curve upon normalization by N^2 . The solid line represents the grafting density variation predicted by eq 16; the deflections follow this scaling law once moderate grafting densities are reached. Similar trends are seen using the SF calculations. The agreement among these results suggests that these methods can be used to estimate the effects of conformational entropy, even for the short chains we consider. The deflections predicted by the different algorithms are compared in Figure 5b. These values are several orders of magnitude smaller than those seen experimentally for ssDNA (see Figures 2 and 3 in Wu et al.²). These results demonstrate that conformational entropy alone is not sufficient to account for the deflections observed for ssDNA.

When considering polyelectrolytes with weak (hard sphere only) segment–segment interactions (thus no hydration forces), we discovered that the dominant force determining deflections originated from F_{OSM} . We can show this explicitly by comparing the forces that result from the polymer and osmotic free energies. These forces are obtained by differentiating eqs 14 and 19 with respect to R :

$$\frac{\partial F_{\text{POLY}}}{\partial R} = \frac{15}{64} \sigma^{13/6} \frac{L_C^2}{R^2} \left(\frac{v}{l}\right)^{2/3} \quad (25)$$

and

$$\frac{\partial F_{\text{OSM}}}{\partial R} = -\left(\frac{L}{R}\right)^2 \left\{ n^\infty \frac{K^2(K(1+K^2)^{-1/2} - 1)}{Q} + \left[1 - n^\infty \left(Q + \frac{1}{Q}\right) \right] \ln \left[\frac{1 - n^\infty \left(Q + \frac{1}{Q}\right)}{1 - 2n^\infty} \right] + K[K(1+K^2)^{-1/2} - 1] \left(1 - \frac{1}{Q^2} \right) n^\infty \left[1 + \ln \left[\frac{1 - n^\infty \left(Q + \frac{1}{Q}\right)}{1 - 2n^\infty} \right] \right] \right\} \quad (26)$$

In the limit of $R \gg L$, eq 15 indicates that $L \sim L_C$. Thus we see that the variations of both the conformational and osmotic free energies scale as L_C^2 , which means whatever conclusion we draw from the following analysis should apply at any chain length. The relative magnitude of the two forces is shown in Figure 6 as a function of grafting density. Note that the counterion osmotic force is an order of magnitude larger than the polymer force at all grafting densities considered. We cannot use eq 26 at grafting densities above 0.1 chains/nm² because the concentration of counterions becomes large enough that the ideal gas approximation for the free energy of the counterions becomes invalid.

SF calculations are valid at higher grafting densities. However, we cannot explicitly compare the contribution of different forces as was done above because there are no analytic expressions for individual effects. Instead, we can compare deflections predicted for flexible chains to those obtained for rods. Since the rods have no conformational freedom, all of the deflection in this limit must result from counterion osmotic pressure. Figure 7 shows the deflections predicted using the SF method; note that the deflections predicted for rods are actually slightly higher. This is because, on average, the counterions are located closer to the surface of the cantilever for flexible chains, where brush heights are smaller than the contour length due to conformational entropy. Thus, bending of the cantilever results in less of an increase in available volume for counterions in the case of flexible chains, as compared to a system of rodlike chains. Our calculations show that the increase in conformational entropy with curvature for flexible chains is unimportant compared to the increase in configurational entropy of the counterions due to bending of the cantilever. Using the SF algorithm, the persistence length can be varied from one segment up to the entire chain length (rod). As this is done, the deflection monotonically increases because the brush height is increasing. The chain conformational entropy contribution is indeed decreasing as this occurs, but this contribution is less important.

Before accepting this result, we should discuss the significance of electrostatic repulsions in these calculations. The PB expression assumes that the electrostatic repulsions can be accounted for by eq 17, and the SF calculation makes a mean field approximation parallel to the cantilever surface. This effectively smears charge within each horizontal layer, so it is possible that the effect of electrostatic repulsions is underrepresented in both methods. For this reason, we carried out MC simulations with a repulsive potential ($u(r)$) representative of screened electrostatic repulsions:

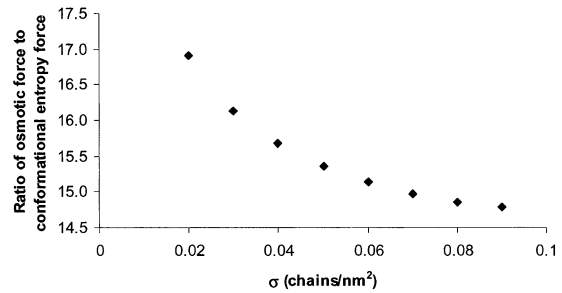


Figure 6. Ratio of the counterion and conformational entropy contributions. The ratio of $(\partial F_{\text{OSM}}/\partial R)/(\partial F_{\text{CONF}}/\partial R)$ is shown vs grafting density for 0.2 M NaCl and $L_C = 15$ nm, with $l_p = 1.5$ nm. The results suggest that the counterion osmotic pressure is significantly more important at all relevant grafting densities, although configurational entropy effects have a higher scaling dependence on grafting density. Because excluded volume of the counterions is neglected in eq 26, it is not applicable to higher grafting densities.

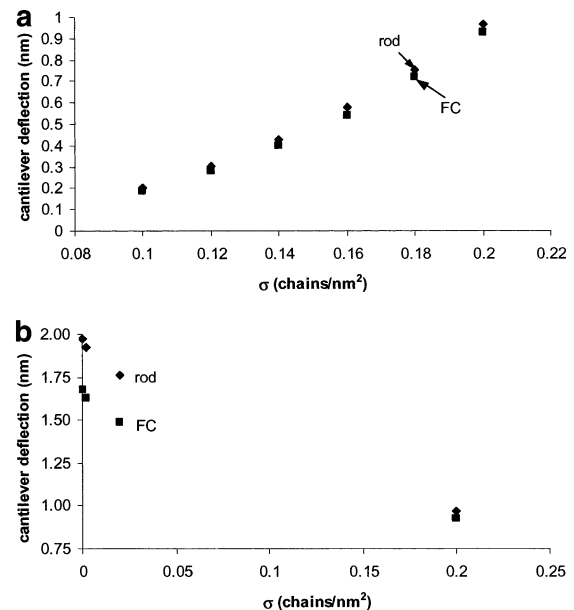


Figure 7. Comparison of deflections predicted by the SF method for rods and flexible chains (denoted as FC) in the screened electrostatic regime for $L_C = 15$ nm. At all grafting densities the deflections are greater for rods. (a) Variation of deflection with grafting density for a bulk salt concentration of 0.2 M. (b) Variation with salt concentration is shown for a grafting density of 0.2 chains/nm².

$$u(r) = u_0 \frac{\exp(-\kappa(r - R_{\text{ion}}))}{r(1 + \kappa R_{\text{ion}})} \quad (27)$$

where r is the distance between monomers, and R_{ion} is the radius of the phosphate ion on the DNA. Equation 27 is an extension of eq 23 that includes finite ion size. In these MC simulations, each monomer corresponds to a bead with a diameter equal to the Bjerrum length, so that $f = 1$. This corresponds to approximately two nucleotides. We took the statistical segment length to be 1.5 nm; thus conformational freedom was allowed only at every second bead. To be carried out properly, these simulations should be coupled to an algorithm that solves the PB equation in order to determine changes in local salt concentration as different polymer conformations are sampled. Since the purpose of these simulations is only to determine the significance of electrostatic repulsions, we assumed a constant salt concentration within the brush and did NOT account for osmotic pressure effects. The deflections which result for an internal salt concentration of 1 M and $R_{\text{ION}} = 0.6$ nm are shown

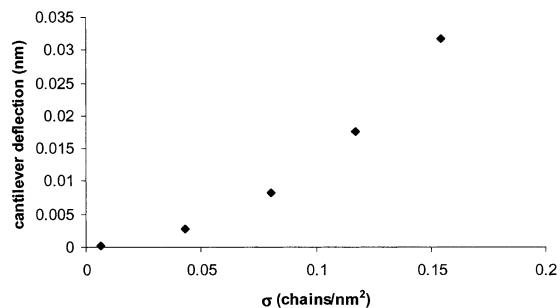


Figure 8. Deflections from MC simulations with screened electrostatic repulsions. Salt concentration (C_S) = 1 M. ssDNA was represented by beads 0.75 nm in diameter, and two beads composed one statistical segment.

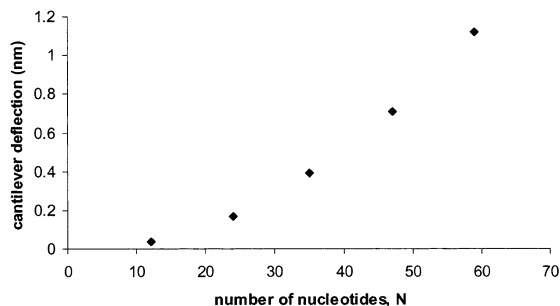


Figure 9. Deflections predicted for using the SF algorithm as a function of chain length. Grafting density is 0.2 chains/nm², and 0.1 M sodium phosphate buffer is simulated. Full Manning condensation is assumed.

in Figure 8. The deflections are much smaller than those that result from counterion osmotic pressure.

SF calculations for chains at the Manning threshold indicate that, regardless of the external salt concentration, the salt concentration within the brush will be comparable to the density of polymer charges for all grafting densities. There is also experimental evidence to corroborate this fact.^{29,33} Thus, we should always expect this screening to occur in our model, which means electrostatic repulsions will contribute a smaller effect than the osmotic pressure in all cases for flexible polyelectrolytes.

The deflections resulting from osmotic pressure for screened polyelectrolytes without hydration forces (Figure 9) are an order of magnitude smaller than those predicted for dsDNA (Figure 3) with hydration forces considered. Note that the deflections in both cases scale as $\delta \sim N^2$, so the comparison can be made at any chain length. Experimental results at higher salt concentration² find that cantilever deflection decreases upon hybridization. The results described in this section demonstrate that effects due to conformational entropy changes and electrostatic interactions alone cannot explain this observation.

2.3.c. Results for Flexible Polymers (ssDNA with Strong Interactions). The results in the preceding section indicate that we cannot obtain experimentally relevant deflections for ssDNA with the physics we have included thus far—we must consider stronger segment–segment interactions. Strongly repulsive segment–segment interactions will cause chains to favor extended conformations. Beyond a certain value of the interaction strength, these conformations will resemble those of a nematic system. If our system of flexible chains is in this regime, it will be desirable to use eq 8 to model them because then we will be able to use the same model for both ssDNA and dsDNA, which facilitates comparisons. Therefore, we performed MC simulations of flexible chains with strong interactions, and we first show that eq 8 is consistent with the results of these

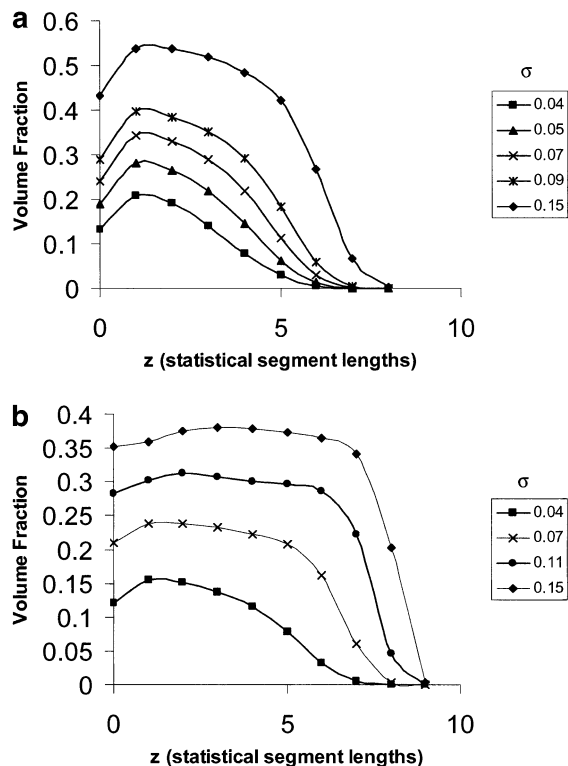


Figure 10. (a) Volume fraction profiles for athermal chains with 10 statistical segments. Results are similar to those obtained using the SF method. (b) Volume fraction profiles for chains with 10 segments with interactions. The profiles for grafting densities larger than 0.07 chains/nm² are significantly different from the parabolic profiles in (a).

simulations. We then discuss how strong the segment–segment interactions in ssDNA need to be for this model to predict the deflections observed experimentally.

The most probable cause of strong repulsive interactions in ssDNA is hydration forces, which we expect to result from similar origins as in dsDNA. Thus, the simulations we will discuss used values of λ that were similar to the correlation length of water. Although we used values of u_0 which correspond to weaker interactions than those seen in dsDNA, the interactions were sufficient to produce an abundance of extended conformations. This can be seen by comparing the volume fraction profiles for chains with strong interactions (Figure 10b) to those for athermal chains (Figure 10a). Note that the profiles for athermal chains show the expected parabolic shape^{22,23} even for chains as short as 5 or 10 segments. The profiles for the strongly interacting chains are much closer to step functions (i.e., an Alexander–De Gennes profile²⁰).

The possibility that we can study strongly repulsive flexible chains using eq 8 can be first analyzed by examining the variation of deflection with λ at different grafting densities. In the limit of small interaxial separations or long decay lengths, the bare interactions will dominate eq 8. As we move away from this limit, the second term begins to take over, and the bare potential is renormalized, eventually quadrupling the effective decay length. If the chains in our simulations behave like chains in a nematic system, our simulation results should exhibit this behavior. In the limit of small curvature and no fluctuations, the deflection resulting from a potential ($u(r)$) described by eq 8 can be written as

$$\ln \delta' \cong \frac{-1}{\lambda \sigma^5} \quad (28)$$

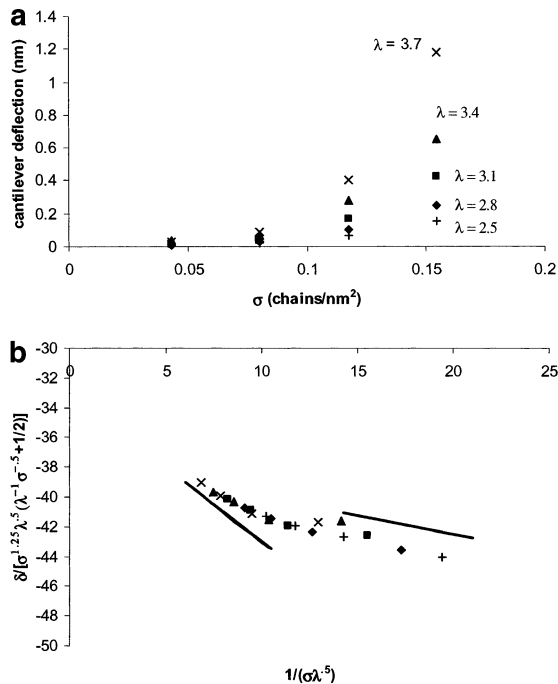


Figure 11. (a) Variation of deflections with λ . The segment–segment interactions are given by eq 23 with $u_0 = 1260 k_B T$ nm/statistical segment, and the values of λ are given in nm. (b) Data are replotted as suggested by eq 28. The lower line describes a slope of -1 and the upper line shows a slope of -0.25 .

where

$$\delta' = \frac{\delta}{\sigma^{1.25} \lambda^{1/2} \left(\frac{1}{\lambda \sigma^{0.5}} + \frac{1}{2} \right)} \quad (29)$$

where we have suppressed some terms which do not vary with grafting density or interaction strength. In the limit where fluctuations dominate, the deflection should still satisfy eq 28, but now λ should be replaced by 4λ .

Figure 11 is a plot of δ' (obtained from MC simulations at different values of λ and σ) against $1/\lambda\sigma^{0.5}$. If the chains behave like a nematic system, we expect the data from different simulations to fall on a single curve. We expect the slope of this curve to be -1 in the region where fluctuations are suppressed and -0.25 in the region where fluctuations dominate (recall the effective decay length is quadrupled). There is clearly a great deal of scatter in the limit of small interaction strength, but the overall slope is close to -0.25 . At higher interaction strengths the normalized deflections appear to approach one line with a slope that is close to -1 .

Deflections predicted by the analysis of Strey et al.⁹ (eq 8) are in quantitative agreement with results from the MC simulations. For a given simulation, all parameters in eq 8 were set except for c , which was treated as an interaction strength dependent fit parameter in Strey et al.⁹ As shown in Figure 12, we find near perfect agreement with the simulation results, provided c increased slightly with interaction strength. In all cases, c is of order 1. Note that the analysis leading to eq 8 assumes the chains are grafted in an ordered, periodic manner, while the chains in our simulations have annealed graft points. Since the chains repel each other strongly, annealing results in surface arrangements that are close to being ordered. Hence, deflections for chains with annealed graft points are very close to those for chains grafted in an ordered fashion (not shown).

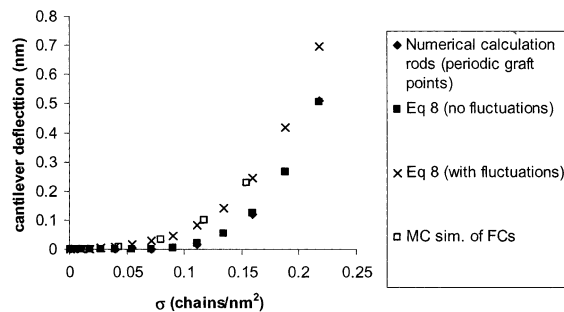


Figure 12. Using eq 8 to predict deflections for the MC chains with strong interactions. Simulation (connected spherical beads) and analytical (cylinders, eq 8) results are shown for flexible chains. As a reference point, the deflections for rods with periodic, ordered graft points are shown for both spherical beads (obtained by numerical integration) and cylinders (obtained using eq 8 with the second term neglected). In the case shown, $u_0 = 630 k_B T$ nm/statistical segment (corresponding to $b = 2.34 \times 10^{-9}$ J/m), $\lambda = 3.1$ Å, and $c = 0.32$. Similar agreement between theory and numerical calculations is found at all values of u_0 and λ studied. The value of c used is independent of σ , but as the deflection increases at a given σ (through increasing u_0 and/or λ) c increases but remains of order 1. The value of c used for the dsDNA interactions in Strey et al.¹⁰ (for salt concentrations greater than 1 M) is 1.2.

The preceding comparison was done only for chains with five segments. However, the MC deflections scaled as $\delta \sim N^2$, as do the deflections predicted by eq 8. Thus the analysis is valid at any chain length. (It can be shown that, in our model, for any system in which the brush height is proportional to N , the deflection will scale with N^2 in the small curvature limit.)

The deflections we have considered thus far in this section are significantly smaller than the experimental values. As the grafting density, u_0 (or b in eq 8), or λ is increased, the predicted deflections increase, but both the theory and simulations indicate that the effect of fluctuations decreases. Once the interactions become strong enough to predict deflections seen experimentally for either dsDNA or ssDNA, the effect of fluctuations is less than 10% at any reasonable persistence length. Thus, assuming that segment–segment interactions are stronger for dsDNA than ssDNA, our calculations always predict a larger cantilever deflection for dsDNA. This is consistent with the experiments by Fritz et al.¹ and inconsistent with the experiments in Wu et al.²

Our conclusion would be different for a “softer” cantilever, in which case the relevant grafting densities are below the threshold at which fluctuations are suppressed. As an example, consider a cantilever for which $C = 0.03$ nJ (33 times smaller than the value used for the experimental cantilever). We computed deflections as a function of persistence length for chains at a grafting density corresponding to $\langle d_0 \rangle = 3.4$ nm, with the interaction potential for dsDNA at 1 M NaCl. Note that this average distance is larger than 3.2 nm, the threshold below which hydration forces dominate and fluctuations are suppressed. We find for $l_p = 1$ nm (ssDNA) $\delta = 35.5$ nm, and for $l_p = 50$ nm (dsDNA) $\delta = 19.5$ nm, and if we assume the dsDNA is too short for fluctuations to be included ($l_p = \infty$), then $\delta = 9.2$ nm. From the standpoint of device design, this points to the importance of the interplay between the mechanical properties of the cantilever and characteristics of target and probe molecules. Changing the cantilever stiffness can lead to observable deflections at much lower adsorbate densities, and a consequent change in even the direction in which the cantilever deflects upon target–probe binding.

2.4. Effect of Nonspecific–Surface Interactions. Nonspecific (i.e., not due to gold–thiol bonds) attractions

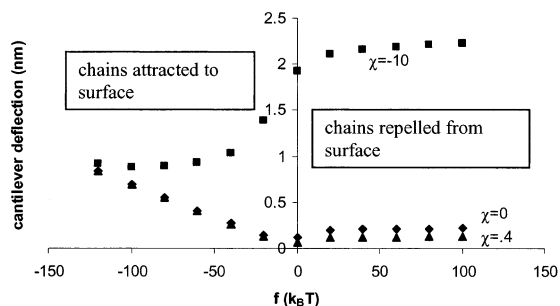


Figure 13. Effect of segment/surface interactions on cantilever deflections predicted using SF algorithm for neutral chains. The attractive potential with the surface is given by: $u(z) = f \exp(-z/\lambda_s)$. Grafting density was 0.06 chains/nm², L_C was 10 nm, the lattice size was 0.667 nm, and $l_p = 1$ nm. In all cases shown, $\lambda_s = 1$ lattice unit. As the Flory χ parameter decreases, the segment–segment interactions become more repulsive.

between DNA and gold have been reported in several experimental investigations; it is assumed they arise from electrostatic attractions to the gold surface.^{34,35} The most important effect of nonspecific interactions is that they may hinder the realization of surfaces with an equilibrium distribution of adsorbed probe molecules. We used SF calculations and Monte Carlo simulations to examine the effect of nonspecific segment/surface interactions given that equilibrium conditions prevail.

Figure 13 shows SF predictions for systems in which surface interactions range from very repulsive to strongly attractive potentials and intersegment interactions are of the excluded volume type. The most relevant observation is that cantilever deflection is not significantly affected by surface interactions unless the interaction strength is very large. The physical reason for the dependence of cantilever deflection on segment/surface interactions is the following. A strongly repulsive potential causes the chains to take extended conformations. The driving force for deflection is the fact that the lateral distance between segments on neighboring chains increases as the cantilever curves. The magnitude of this increase becomes larger as segments move away from the surface. Thus systems with extended conformations experience a larger driving force to deflect. As this potential is decreased and eventually becomes attractive, the chain conformations move closer to the surface, and the deflections decrease.

Once the surface potential becomes attractive, there is a competing effect which favors increased deflections: as the cantilever curves, more polymer segments can approach the surface and experience the favorable surface potential (which decays with distance from the surface). At some point this effect will dominate over segment–segment repulsions. Thus, there is a minimum in deflection at some strength of the attraction, after which a more attractive potential yields larger deflections. MC simulations and electrostatic SF calculations show similar trends.

3. Summary and Conclusions

Inexpensive devices that can rapidly detect pathogens and biological/chemical hazards are highly desirable. One strategy that is being explored toward this end is to exploit microcantilevers with adsorbed probe molecules that deflect upon molecular recognition of target molecules. We have presented a model that examines microcantilever deflections resulting from DNA hybridization. For dsDNA in the regime pertinent to recent experiments,^{1,2} we find that hydration forces are the dominant factor determining cantilever deflections, not electrostatics or conformational entropy. Using an empirical potential¹⁰ derived

from independent experiments, which accounts for these effects, we predict deflections that are consistent with results in Wu et al.² We predict cantilever deflections for the adsorption of ssDNA that are smaller than those for dsDNA, which agrees with the observations in Fritz et al.,¹ but is not consistent with Wu et al.² Our calculations show that, if a more flexible cantilever is considered, experimentally relevant deflections can be achieved at interaction strengths and grafting densities for which conformational entropy is a significant factor. Under these conditions, deflections can be smaller upon hybridization, as seen in Wu et al.² This underscores the importance of considering the interplay between material properties and probe–target interactions during microdevice design.

Our calculations highlight the importance of grafting density in determining the magnitude of cantilever deflections. An important finding is that cantilever deflections are very sensitive to the morphology of the surface, as evidenced by the influence of disordered grafting points on deflection. This emphasizes that characterization and control of nanoscale self-assembly processes that determine probe molecule adsorption are imperative for reliable microdevice design. This suggests that experiments which use techniques such as neutron scattering,³⁶ STM,³⁷ or AFM³⁸ to image the surface are desirable for learning the relationships between surface preparation protocols and controlled self-assembly of adsorbed probe molecules.

Since it is such an important quantity, it may be desirable to relate the grafting density (and corresponding surface stress) to the DNA bulk chemical potential, (e.g., a Gibbs adsorption isotherm calculation). However, due to the irreversible nature of the gold–thiol bond (on experimental time scales) and the large time constant associated with additional chains penetrating the polymer brush once moderate grafting densities are achieved, it is likely that a purely thermodynamic description of the adsorption process is inappropriate.

Finally, we note that our calculations assume that the molecules which have adsorbed are in equilibrium with each other. Nonspecific segment/surface interactions may lead to the formation of nonequilibrium surfaces,³⁶ in which case our calculations are not relevant. Perhaps more importantly, we cannot expect reproducible and reliable results from a microdevice that does not use surfaces annealed under equilibrium conditions. Efforts to prevent realization of nonequilibrium surfaces, including the blocking of nonspecific DNA segment/surface interactions by the introduction of small thiolated molecules,^{34,36,39} should be explored.

Acknowledgment. Financial support for this work was provided by Defense Advanced Research Projects Agency (DARPA/ F30602-01-2-0540). M.F.H. was also supported by a National Science Foundation predoctoral fellowship.

References and Notes

- (1) Fritz, J.; Baller, M. K.; Lang, H. P.; Rothuizen, H.; Vettiger, P.; Meyer, E.; Guntherodt, H.-J.; Gerber, Ch.; Gimzewski, J. K. *Science* **2000**, *288*, 316.
- (2) Wu, G.; Haifeng, J.; Hansen, K.; Thundat, T.; Datar, R.; Cote, R.; Hagan, M. F.; Chakraborty, A. K.; Majumdar, A. *Proc. Natl. Acad. Sci. U.S.A.* **2001**, *98*, 1560.
- (3) Wu, G.; Datar, R. H.; Hansen, K. M.; Thundat, T.; Cote, R. J. Majumdar, A. *Nat. Biotechnol.* **2001**, *19*, 856.
- (4) Hansen, K. M.; Ji, H.-F.; Wu, G.; Datar, R.; Cote, R.; Majumdar, A.; Thundat, T. *Anal. Chem.* **2001**, *73*, 1567.
- (5) (a) Smith, S. B.; Cui, Y.; Bustamante, C. *Science* **1996**, *271*, 795. (b) Baumann, C. G.; Smith, S. B.; Bloomfield, V. A.; Bustamante, C. *Proc. Natl. Acad. Sci. U.S.A.* **1997**, *94*, 6185.
- (6) (a) Cheatham, T. E. III; Kollman, P. A. *Annu. Rev. Phys. Chem.* **2000**, *51*, 435. (b) Beveridge, D. L.; McConnel, K. J. *Curr. Opin. Struct.*

- Biol.* **2000**, *10*, 182. (c) Zeng, J.; Wang, X.; Krull, U. J. *Proc. SPIE (International Conference on Sensor Technology ISTC 2001)* **2001**, *4414*, 1.
- (7) Ibach, H. *Surf. Sci. Rep.* **1997**, *29*, 193.
- (8) Peterson, A. W.; Heaton, R. J.; Georgiadis, R. M. *Nucleic Acids. Res.* **2001**, *29*, 5163.
- (9) Strey, H. H.; Parsegian, V. A.; Podgornik, R. *Phys. Rev. E* **1999**, *59*, 999.
- (10) Strey, H. H.; Parsegian, V. A.; Podgornik, R. *Phys. Rev. Lett.* **1997**, *78*, 895.
- (11) Podgornik, R.; Parsegian, V. A. *Macromolecules* **1990**, *23*, 2265.
- (12) Podgornik, R.; Rau, D. C.; Parsegian, V. A. *Biophys. J.* **1994**, *66*, 962.
- (13) Rau, D. C.; Lee, B.; Parsegian, V. A. *Proc. Natl. Acad. Sci. U.S.A.* **1984**, *81*, 2621.
- (14) Brenner, S. L.; Parsegian, V. A. *Biophys. J.* **1974**, *14*, 327.
- (15) (a) Manning, G. S. *J. Chem. Phys.* **1969**, *51*, 924. (b) Manning, G. S. *J. Chem. Phys.* **1969**, *51*, 3249. (c) Oosawa, F. *Polyelectrolytes*; Marcel Dekker: New York, 1971. (d) Muthukumar, M. *J. Chem. Phys.* **1996**, *105*, 5183. (e) Patra, C. N.; Yethiraj, A. *J. Phys. Chem. B* **1999**, *103*, 6080.
- (16) Hansen, P. L.; Podgornik, R.; Parsegian, V. A. *Phys. Rev. E* **2001**, *64*, 021907.
- (17) Leiken, S.; Parsegian, V. A.; Rau, D. C.; Rand, R. P. *Annu. Rev. Phys. Chem.* **1993**, *44*, 369.
- (18) Saenger, W. *Principles of Nucleic Acid Structure*; Springer-Verlag: New York, 1984; Chapter 17.
- (19) Steel, A. B.; Levicky, R. L.; Herne, T. M.; Tarlov, M. J. *Biophys. J.* **2000**, *79*, 975.
- (20) (a) Alexander, S. *J. Phys. (Paris)* **1977**, *38*, 977. (b) Alexander, S. *J. Phys. (Paris)* **1977**, *38*, 983. (c) De Gennes, P. G. *Macromolecules* **1980**, *13*, 1069.
- (21) Granick, S.; Patel, S.; Tirrell, M. *J. Chem. Phys.* **1986**, *85*, 5370.
- (22) Milner, S. T.; Witten, T. A.; Cates, M. E. *Macromolecules* **1988**, *21*, 2610.
- (23) Flerer, G. J.; Cohen Stuart, M. A.; Scheutjens, J. M. H. M.; Cosgrove, T.; Vincent, B. *Polymers at Interfaces*; Chapman and Hall: London, 1993.
- (24) Daoud, M.; Cotton, J. *J. Chem. Phys.* **1982**, *43*, 531.
- (25) Halperin, A. *Macromolecules* **1987**, *20*, 2943.
- (26) Tinland, B.; Pleun, A.; Sturm, J.; Weill, G. *Macromolecules* **1997**, *30*, 5763.
- (27) Hiergiest, C.; Lipowsky, R. *J. Phys. II Fr.* **1996**, *6*, 1465.
- (28) Pincus, P. *Macromolecules* **1991**, *24*, 2912.
- (29) Harharan, R.; Biver, C.; Russel, W. B. *Macromolecules* **1998**, *31*, 7514.
- (30) Bohmer, M. R.; Koopal, L. K.; Lyklema, J. *J. Phys. Chem.* **1991**, *95*, 9569.
- (31) (a) Leermakers, F. A. M.; Scheutjens, J. M. H. M. *J. Phys. Chem.* **1989**, *93*, 7417. (b) Leermakers, F. A. M.; Lyklema, J. *Colloids Surf.* **1992**, *67*, 239. (c) Wijmans, C. M.; Leermakers, F. A. M.; Flerer, G. J. *J. Chem. Phys.* **1994**, *101*, 8214.
- (32) Frenkel, D.; Mooij, G. C. A. M.; Smit, B. *J. Phys.: Condens. Matter* **1991**, *3*, 3053.
- (33) Balastre, M.; Li, F.; Schorr, P.; Yang, J.; Mays, J. W.; Tirrell, M. V. *Macromolecules*, in press.
- (34) Satjapipat, M.; Sanedrin, R.; Zhou, F. *Langmuir* **2001**, *17*, 7637.
- (35) Georgiadis, R.; Peterlinz, K. P.; Peterson, A. W. *J. Am. Chem. Soc.* **2000**, *122*, 3166.
- (36) Levicky, R.; Herne, T. M.; Tarlov, M. J.; Satija, S. K. *J. Am. Chem. Soc.* **1998**, *120*, 9787.
- (37) Rekes, D.; Lyubchenko, Y.; Shlyakhtenko, L. S.; Lindsay, S. M. *Biophys. J.* **1996**, *71*, 1079.
- (38) Csaki, A.; Moller, R.; Straube, W.; Kohler, J. M.; Fritzsche, W. *Nucleic Acids. Res.* **2001**, *29*, e81.
- (39) Peterlinz, K. A.; Georgiadis, R. M. *J. Am. Chem. Soc.* **1997**, *119*, 3401.